

Chapter 2

The CMS Experiment at the LHC

The Large Hadron Collider (LHC) [1] is designed to collide proton beams at a center-of-mass energy of $\sqrt{s} = 14 \text{ TeV}$ and a nominal instantaneous luminosity of $\mathcal{L} = 10^{34} \text{ cm}^{-2}\text{s}^{-1}$. This represents a seven-fold increase in energy and a hundred-fold increase in integrated luminosity over the previous hadron collider experiments. The beam energy and the design luminosity have been chosen in order to study physics at the TeV energy scale. The main motivation of the LHC is to reveal the nature of electroweak symmetry breaking and to investigate potential manifestations of new physics phenomena beyond the SM.

The unprecedented high center-of-mass energy and luminosity at the LHC lead to a number of substantial experimental challenges. In this chapter an introduction of the experimental facility is presented. An overview of the basic aspects of the LHC is followed by a detailed description of the CMS experiment and its main subdetectors.

2.1 The Large Hadron Collider

The LHC accelerator is located at CERN near Geneva in the already existing LEP tunnel which has a length of 26.7 km. Four detectors are installed in the experimental caverns around the collision points: Two general purpose experiments, ATLAS [2] and CMS [3, 4], the LHCb [5] experiment dedicated to B Physics and the ALICE [6] experiment where the physics of heavy ion collisions is investigated.

To supply the LHC with pre-accelerated protons the existing CERN facilities have been upgraded. A schematic view of the LHC accelerator with the injection chain is shown in Fig. 2.1. The protons coming from the Super Proton Synchrotron (SPS) with an energy of 450 GeV are injected into the LHC, where they will be accelerated to an energy of 7 TeV in bunches with a nominal number of $1.15 \cdot 10^{11}$ particles per bunch. Superconducting dipole magnets which provide a magnetic field of 8.3 T are needed to keep the protons on the orbit during the acceleration. The superconducting magnets are cooled using liquid helium at a temperature of 1.9 K.

At the interaction point where the CMS experiment is located collisions happen every 25 ns, corresponding to a bunch crossing frequency of 40 MHz. The total proton-proton cross section at $\sqrt{s} = 14$ TeV is expected to be about 100 mb. Therefore, approximately 10^9 inelastic events per second will be observed in the multi-purpose experiments at design luminosity.

In the first year of LHC running the proton-proton collisions happen at a lower center-of-mass energy of $\sqrt{s} = 7$ TeV and at a lower luminosity than what is foreseen in the original design. A commissioning run with collisions at center-of-mass energies of $\sqrt{s} = 900$ GeV and 2.36 TeV took place in November and December 2009. The LHC operation at $\sqrt{s} = 7$ TeV started on March 30, 2010.

2.2 The CMS Detector

The CMS detector is a general purpose detector installed 100 m underground at the LHC interaction point 5 (P5) near the village of Cessy in France. The design of the CMS detector is driven by the challenges of a physics experiment in the LHC environment. Many of the physics benchmark channels have a small cross section and the background from QCD jet production is overwhelmingly dominant. A high rejection power with an optimal efficiency for rare channels has to be achieved. The reconstruction of lepton signatures is essential for the extraction of rare processes and an excellent muon and electron identification and momentum resolution is desired. Moreover, a precise measurement of secondary vertices and impact parameters is necessary for an efficient identification of heavy flavor and τ -lepton decays.

The short bunch crossing separation and the high event rate at the LHC impose further challenges to the design. At design luminosity, 23 inelastic interaction per bunch crossing will occur on average. This phenomenon is known as pile-up. The effect of pile-up can be reduced by using high-granularity detectors resulting in low occupancy. This requires a large number of detector channels and an excellent synchronization among them. In addition, a good time resolution is needed to discriminate the interaction under study from the interactions occurring in neighboring bunch crossings. Another difficulty arises from the large flux of particles near the interaction point which leads to high radiation levels and the need of radiation hard detectors and front-end electronics.

The CMS detector is divided into a silicon tracking system, an electromagnetic and a hadronic calorimeter and a muon system. A magnetic field of 3.8 T is provided by a superconducting solenoid magnet. The CMS detector is 22 m long, has a diameter of 15 m and an overall weight of 12.5 t. Figure 2.2 presents a schematic view of the CMS detector.

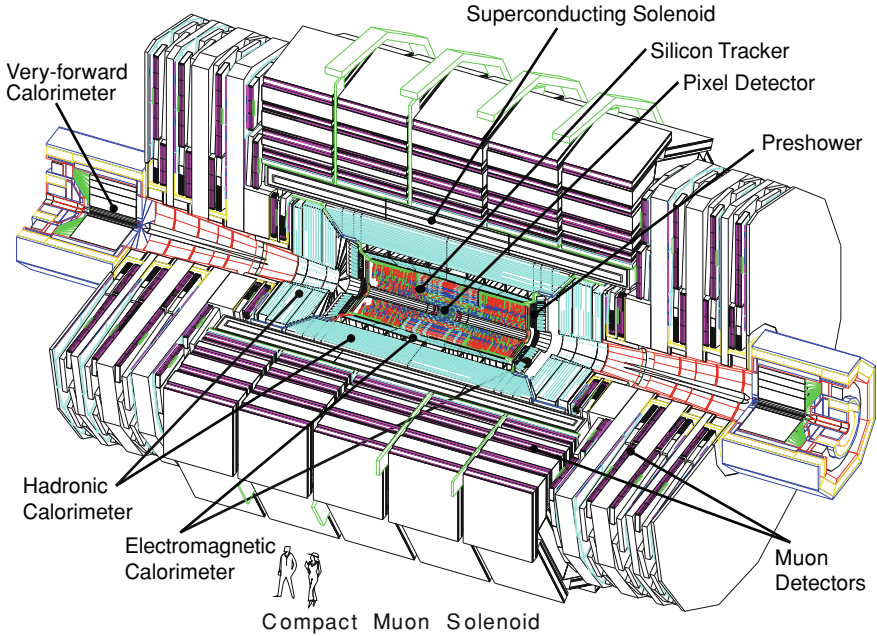


Fig. 2.2 Schematic view of the CMS detector

of the beam to the west. The azimuthal angle ϕ is measured from the x -axis in the xy plane and the radial coordinate in this plane is denoted by r . The polar angle θ is defined in the rz plane and the pseudorapidity is $\eta = -\ln \tan(\theta/2)$. The momentum component transverse to the beam direction, denoted by p_T , is computed from the x - and y -components, while the transverse energy is defined as $E_T = E \sin \theta$.

2.2.2 Solenoid

A superconducting solenoid magnet with a maximum magnetic field of 3.8 T provides the large bending power for high-energy charged particles to precisely measure their momentum in the tracking detectors. The magnetic coil is 13 m long, has an inner diameter of 6 m and accommodates the tracking and part of the calorimeter detectors. With these dimensions the CMS solenoid is the largest superconducting magnet ever built and has the capacity to store an energy of 2.6 GJ at full current. The magnetic flux is returned through a 10,000 t iron yoke in which the muon detector chambers are integrated. The CMS solenoid was fully tested and commissioned at the experimental surface hall during autumn 2006.

2.2.3 Tracking Detectors

CMS features an all silicon tracker with a total active area of 200 m^2 . The tracking detector is divided into a pixel detector close to the interaction region and a strip detector covering radii between 0.2 and 1.2 m. At LHC design luminosity more than 1,000 particles are expected to traverse the tracking volume in each bunch crossing. This leads to a hit rate density of 1 MHz/mm^2 at a radius of 4 cm which imposes severe challenges to the design of the tracking detectors. With a pixel size of $100 \times 150\text{ }\mu\text{m}^2$ an occupancy of less than 10^{-4} can be maintained in the pixel detector. As the particle flux decreases with the distance from the interaction point, sensors with a length of 10 cm and a pitch of $80\text{ }\mu\text{m}$ can be used at intermediate radii (20–55 cm) and sensors with a length of 25 cm and a pitch of $180\text{ }\mu\text{m}$ at the outermost radii (55–110 cm) with an occupancy of less than 3%. The sensor thickness is $285\text{ }\mu\text{m}$ for the pixel and 320 or $500\text{ }\mu\text{m}$ for the strip modules at the intermediate and outer radii, respectively. The thicker sensors for the outer tracking region permit to preserve a signal to noise ratio well above 10 in spite of the higher noise due to the larger capacity of the longer strips. To mitigate the radiation damage effects and prolong the lifetime of the detector modules, the tracking detectors are designed to run at subzero temperatures. The cooling is established using a mono-phase liquid cooling system with C_6F_{14} as cooling fluid.

The pixel detector is built from 3 barrel layers at radii of 4.4, 7.3 and 10.2 cm and two end disks on each side at a distance of $z = \pm 34.5, \pm 46.5\text{ cm}$ from the interaction point. It consists of 1,440 segmented silicon sensor modules with a total of 66 million readout channels. For each pixel the analog pulse height information is detected and read out.

The sensor surface of the barrel modules is parallel to the magnetic field, while the modules in the forward detector are tilted by 20° . The charge carriers produced by a particle traversing the sensor thus experience the Lorentz force and do not drift along the electric field line anymore. Hence, the charge carriers are distributed over several pixels. The analog pulse height information can be used to calculate a center of gravity of the charge distribution which improves the hit information. In this way a position resolution of about $15\text{ }\mu\text{m}$ in both the $r\phi$ and z directions is obtained (compare to Fig. 2.6). A detailed description of the design and the functioning of the CMS pixel barrel detector is given in Chap. 7.

The silicon strip tracker has a length of 5.8 m and a diameter of 2.4 m and is composed of four subsystems: the four-layer Tracker Inner Barrel (TIB), the six-layer tracker outer barrel (TOB) and on each side three-disk Tracker Inner Disks (TID) and nine-disk Tracker Endcaps (TEC). An rz -view of the tracker geometry is shown in Fig. 2.3.

The silicon strip tracker is built from 15,148 single-sided modules that provide 9.3 million readout channels. Modules for the TIB, the TID and the first four rings of the TEC are single-sided while the TOB and the outer three rings of the TEC are equipped with double-sided modules. A double-sided module is constructed from two single-sided modules glued back-to-back at a stereo angle of 100 mrad .

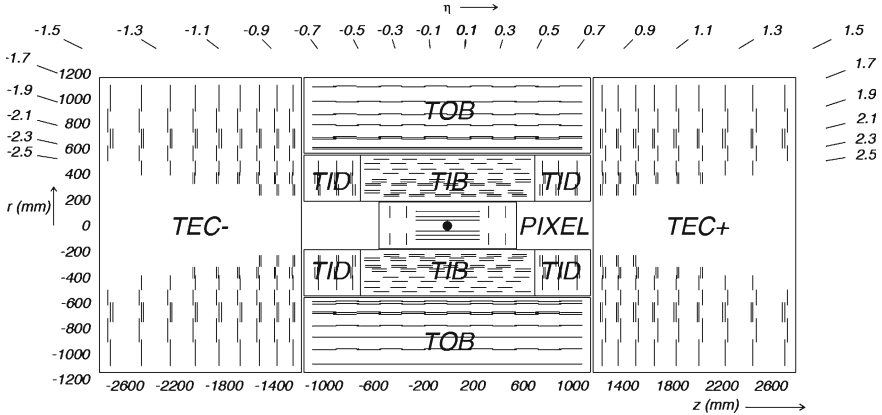


Fig. 2.3 rz -view of the CMS tracking detectors [4]. *Single lines* represent layers of modules equipped with one sensor, *double lines* indicate layers with back-to-back modules

2.2.4 Track Reconstruction

Due to the magnetic field charged particles travel through the tracking detectors on a helix trajectory which is described by 5 parameters: the curvature κ , the track azimuthal angle ϕ and polar angle η , the signed transverse impact parameter d_0 and the longitudinal impact parameter z_0 . The transverse (longitudinal) impact parameter of a track is defined as the transverse (longitudinal) distance of closest approach of the track to the primary vertex.

The main standard algorithm used in CMS for track reconstruction is the Combinatorial Track Finder (CFT) algorithm [7] which uses the reconstructed positions of the passage of charged particles in the silicon detectors to determine the track parameters. The CFT algorithm proceeds in three stages: track seeding, track finding and track fitting. Track candidates are best seeded from hits in the pixel detector because of the low occupancy, the high efficiency and the unambiguous two-dimensional position information.

The track finding stage is based on a standard Kalman filter pattern recognition approach [8] which starts with the seed parameters. The trajectory is extrapolated to the next tracker layer and compatible hits are assigned to the track on the basis of the χ^2 between the predicted and measured positions. At each stage the Kalman filter updates the track parameters with the new hits. In order to take into account possible inefficiencies one further candidate is created without including any hit information. The tracks are assigned a quality based on the χ^2 and the number of missing hits and only the best quality tracks are kept for further propagation. Ambiguities between tracks are resolved during and after track finding. In case two tracks share more than 50% of their hits, the lower quality track is discarded.

For each trajectory the finding stage results in an estimate of the track parameters. However, since the full information is only available at the last hit and constraints

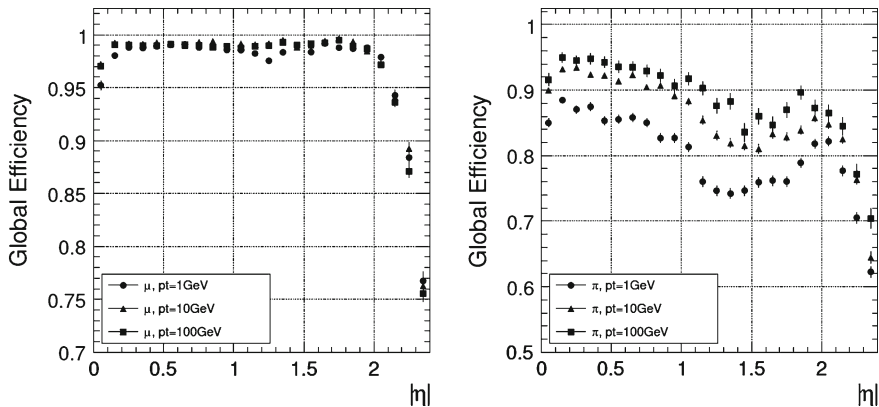


Fig. 2.4 Track reconstruction efficiency for muons (*left*) and pions (*right*) with transverse momenta of 1, 10 and 100 GeV [4]

applied during trajectory building can bias the estimate of the track parameters, all valid tracks are refitted with a standard Kalman filter and a second filter (smoother) running from the exterior towards the beam line.

The expected performance of the track reconstruction is shown in Fig. 2.4 for muons, pions and hadrons. The track reconstruction efficiency for high energy muons is about 99% and drops at $|\eta| > 2.1$ due to the reduced coverage of the forward pixel detector. For pions and hadrons the efficiency is in general lower because of interactions with the material in the tracker. The material budget of the CMS tracker in units of radiation length¹ is presented in Fig. 2.5.

In Fig. 2.6 the transverse momentum resolution for muon tracks with $p_T = 1, 10$ and 100 GeV is shown. At high momenta the resolution is around 1–2% for $|\eta| < 1.6$. The material of the tracker accounts for 20–30% of the transverse momentum resolution. At lower momenta, the resolution is dominated by multiple scattering and its distribution reflects the amount of material traversed by the track. The resolution of the track impact parameters in the longitudinal and the transverse plane are also shown in Fig. 2.6. At high momentum the transverse impact parameter resolution is fairly constant and is dominated by the hit resolution in the first pixel layer. It is progressively degraded by multiple scattering at lower momenta. The same applies to the longitudinal impact parameter resolution. The improvement of the z_0 resolution up to $|\eta| = 0.5$ is due to the charge sharing effects among neighboring pixels.

2.2.5 Electromagnetic Calorimeter

The CMS electromagnetic calorimeter (ECAL) is a hermetic and homogeneous detector with a large pseudorapidity coverage up to $|\eta| < 3$. The ECAL is divided

¹ The radiation length X_0 is a characteristic of a material, related to the energy loss of high energy electrons in the material.

Fig. 2.5 Material budget of the CMS tracker in units of radiation length X_0 as a function of pseudorapidity divided into the contributions of the different subdetectors [4]

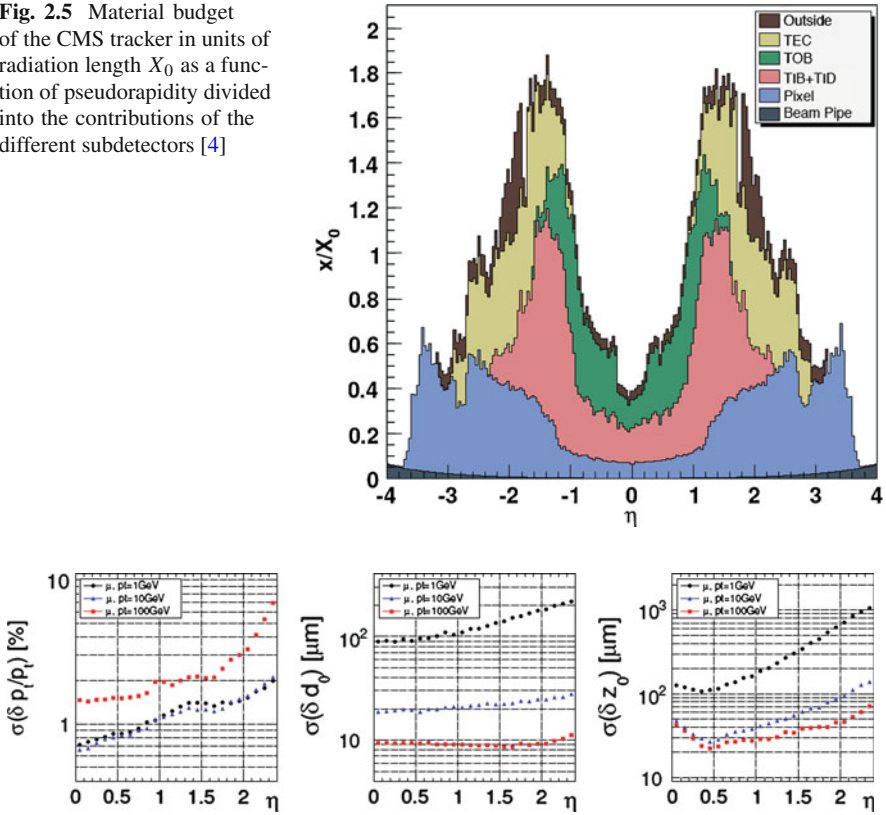


Fig. 2.6 Resolution of track transverse momentum (*left*), transverse impact parameter (*middle*) and longitudinal impact parameter (*right*). The resolution is shown for muons with transverse momenta of 1, 10 and 100 GeV [4]

into barrel and endcap detectors as illustrated in Fig. 2.7. Scintillation crystals made from lead tungstate (PbWO_4) are used to measure the energy of electromagnetically interacting particles, mainly electrons and photons. The choice of PbWO_4 as the material for the scintillation crystal is motivated by its fast response time and high radiation resistance. The ECAL consists of 61,200 crystals in the barrel and 7,324 crystals in the endcaps. The crystals have a tapered shape and are mounted in a quasi-projective geometry. With a crystal front face of $22 \times 22 \text{ mm}^2$ and $28.6 \times 28.6 \text{ mm}^2$ in the barrel and the endcaps, respectively, a fine granularity is ensured. The length of a barrel crystal is 23 cm which corresponds to $25.8 X_0$, while the endcap crystals are 22 cm long corresponding to $24.7 X_0$. The scintillation light produced in the crystals is read out by avalanche photo diodes (APD) with an active area of $5 \times 5 \text{ mm}^2$ in the barrel and by vacuum phototriodes (VPT) with an active area of 280 mm^2 in the endcaps. The light output and the amplification have a strong temperature dependence. The response to an incident electron changes by $(3.8 \pm 0.4)\% / ^\circ\text{C}$ which in

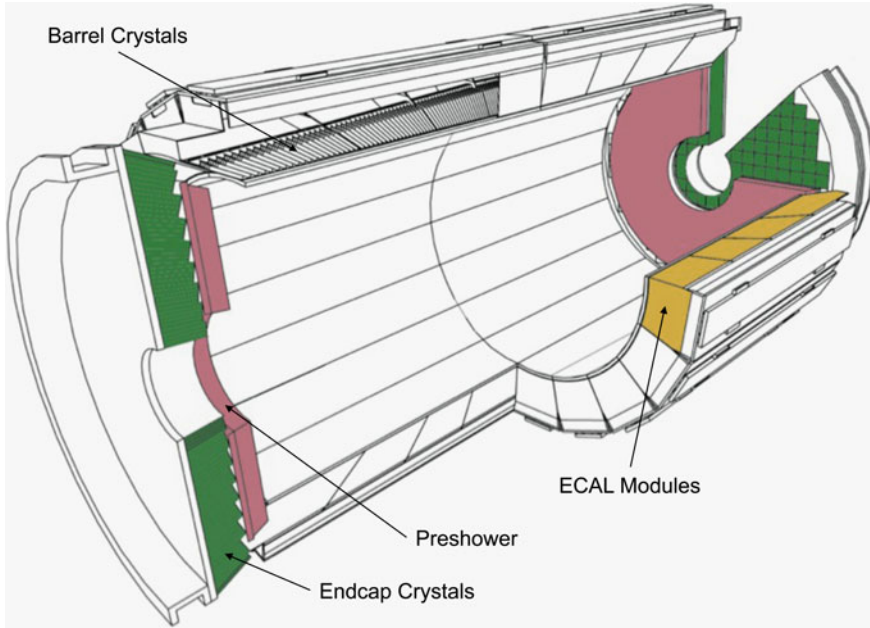


Fig. 2.7 Schematic view of the CMS Electromagnetic Calorimeter [4]

turn means that the temperature has to be closely monitored and kept stable to a precision of $\pm 0.05^\circ\text{C}$. The nominal operating temperature of the ECAL is 18°C and is provided by a water cooling system.

The ECAL barrel has a volume of 8.14 m^3 and its front face is at a radial distance of 1.29 m from the interaction point. It has a 360-fold azimuthal segmentation and two times 85-fold segmentation in pseudorapidity. The endcap has a coverage of $1.479 < |\eta| < 3$ and is situated at a longitudinal distance of 3.15 m from the interaction point. A preshower detector with a thickness of $3 X_0$ is placed in front of the endcaps ($1.653 < |\eta| < 2.6$) to guarantee a reliable discrimination of single photons and photons produced in pairs in neutral pion decays.

The energy resolution of the electromagnetic calorimeter can be parametrized by the following expression:

$$\left(\frac{\sigma}{E}\right)^2 = \left(\frac{S}{\sqrt{E}}\right)^2 + \left(\frac{N}{E}\right)^2 + C^2 \quad (2.1)$$

where S is the stochastic term, N the noise term and C the constant term. The value of the three parameters were determined by a electron test beam measurement to be $S = 0.028\text{ GeV}^{\frac{1}{2}}$, $N = 0.12\text{ GeV}$ and $C = 0.003$. The ECAL energy resolution as a function of the energy of electrons is shown in Fig. 2.8.

Fig. 2.8 ECAL energy resolution as a function of the energy measured in an electron test beam [4]. The measured values of the stochastic (S), noise (N) and constant (C) term are displayed in the legend

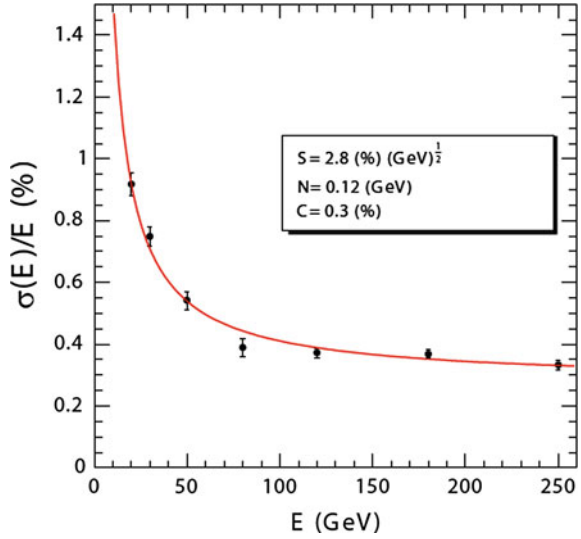


Table 2.1 Tower segmentation in azimuthal and polar angle for the hadronic barrel, endcap and forward calorimeter

	HB/HO	HE $ \eta \leq 2.5$	HE $ \eta > 2.5$	HF $ \eta \leq 4.7$	HF $ \eta > 4.7$
$\Delta\phi \times \Delta\eta$	0.087×0.087	0.087×0.087	0.175×0.175	0.175×0.175	0.175×0.35

2.2.6 Hadronic Calorimeter

The energy measurement of the ECAL is complemented by the measurement of the hadronic calorimeter (HCAL). The HCAL is a sampling calorimeter built from alternating layers of massive absorbing brass plates and plastic scintillator tiles arranged in trays. The quality of the energy measurements depends on the fraction of the hadronic shower detected in the calorimeter. Consequently, the thickness of the material in the tray has to be large enough to absorb the major part of the shower. The dimensions of the barrel part of the HCAL however are restricted to the limited volume between the outer extent of the ECAL ($r = 1.77$ m) and the inner extent of the magnetic coil ($r = 2.95$ m). Thus, the HB is supplemented by an outer hadronic calorimeter (HO) located between the solenoid and the muon detectors. The HO uses the solenoid as additional absorbing material and provides sufficient containment for hadronic showers with a thickness of 11.8 interaction lengths (λ_I). The hadronic calorimeter is divided into a barrel part (HB and HO) at $|\eta| < 1.3$, an endcap (HE) on each side at $1.3 < |\eta| < 3$ and a forward calorimeter (HF) extending up to $|\eta| < 5.2$ to achieve a most hermetic detector coverage. The HCAL tower segmentation in the rz plane for one quarter of the HB, HO and HE detectors is shown in Fig. 2.9 and summarized in Table 2.1.

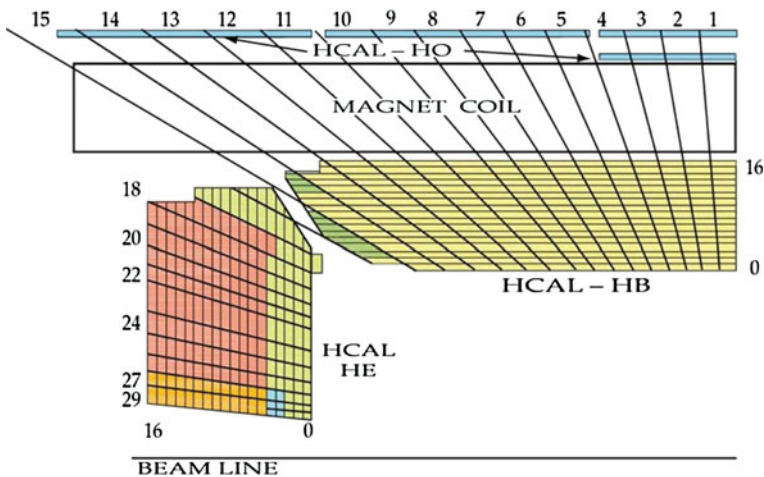


Fig. 2.9 Tower segmentation for one quarter of the HCAL displayed in the rz plane [4]. The colors represent the optical grouping of scintillator layers into different longitudinal readouts

The plastic scintillator tiles are read out by wavelength shifting fibers that shift the blue-violet light emitted by the scintillator to green light which is then sent through transparent fibers to hybrid photodetectors (HPDs) with 19 independent pixels. The first scintillators are placed in front of the first absorber plate in order to sample showers developing in the material between the ECAL and the HCAL, while the last scintillators are installed after the last absorber plate to correct for late developing showers leaking out. 70,000 and 20,916 scintillator tiles are installed in the HB and the HE, respectively.

The HF is positioned at a longitudinal distance of 11.2m from the interaction point. It will experience unprecedented particle fluxes with an energy of 760 GeV deposited on average in a proton-proton interaction at $\sqrt{s} = 14$ TeV. This energy has to be compared to the average of 100 GeV deposited in the rest of the detector. The situation is even more severe as the energy is not spread equally among the HF, but has a pronounced peak at the highest rapidity. The HF is made from steel absorber plates composed of 5 mm thick grooved plates with quartz fibers inserted as active medium. It detects the Cherenkov light emitted by charged particles in the shower and is thus mainly sensitive to the electromagnetic component of the shower. A longitudinal segmentation in two parts allows to distinguish signals generated by electrons and photons from signals generated by hadrons.

2.2.7 Muon System

The muon system is the outermost part of the CMS detector. The magnet return yoke is equipped with gaseous detector chambers for muon identification and momentum measurement. In the barrel, the muon stations are arranged in five separate iron wheels

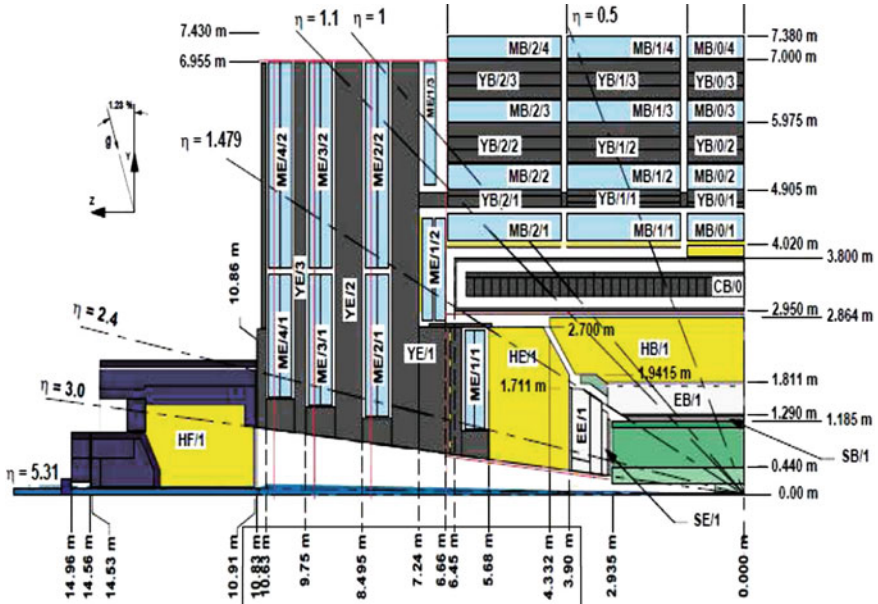


Fig. 2.10 View of one quarter of the CMS detector illustrating the layout of the muon system in the barrel and the endcap region [4]

and in the endcap, four muon stations are mounted onto the three independent iron disks in the positive and the negative endcaps. Each barrel wheel is segmented into 12 sectors in azimuthal angle.

Three different types of gaseous detectors are integrated into the CMS muon system depending on the requirements. In the barrel part where both the muon rate and the neutron induced background are small and the magnetic field is very low, drift tube (DT) chambers are used. In the endcaps however the muon and the background flux is much higher. The muon detector endcaps are thus built from cathode strip chambers (CSCs) which provide a faster response, a higher granularity and a better resistance against radiation. In addition, resistive plate chambers (RPCs) form a redundant trigger system. In total, the CMS muon system consists of 250 DT chambers, 540 CSCs and 610 RPCs. The arrangement of the detector chambers is shown in Fig. 2.10.

A DT cell is a 4 cm wide gas tube with a positively charged stretched wire inside. Each DT chamber, on average 2×2.5 m in size, consists of 12 layers of DT cells, arranged in three groups of four. The middle group measures the z coordinate while the two outside groups measure the $r\phi$ coordinate. In the barrel, four DT chambers are interspersed with the layers of the flux return yoke in each ϕ sector. The outermost muon station is equipped with DT chambers that contain only 8 layers of DT cells and determine the muon position in the $r\phi$ plane. The barrel part of the muon system covers the region $|\eta| < 1.2$.

The CSCs are trapezoidal shaped multiwire proportional chambers which consist of 6 anode wire planes crossed with 7 copper strips cathode panels in a gas volume. They provide a two-dimensional position measurement, where the r and ϕ coordinates are determined by the copper strips and the anode wires, respectively. The muon detector endcaps consist of 4 CSC stations on each side and identify muons in the pseudorapidity range of $0.9 < |\eta| < 2.4$.

RPCs are made from two high resistive plastic plates with a voltage applied and separated by a gas volume. The signal generated by the muon when passing through the gas volume is detected by readout strips mounted on top of one of the plastic plates. The RPCs used in the muon trigger system are highly segmented and have a fast response with a time resolution of 1 ns. Six layers of RPCs are installed in the barrel muon system, two layers in each of the first two stations and one layer in each of the last two stations. One layer of RPCs is built into each of the first three stations of the endcap.

2.2.8 Muon Reconstruction

Muon reconstruction, after local-pattern recognition is performed in two stages: stand-alone reconstruction based on information from the muon system only and global reconstruction including the hit information of the silicon tracker. Stand-alone reconstruction starts from track segments in the muon chambers and muon trajectories are built from the inside to the outside using the Kalman filter technique. After the trajectory is built, a second Kalman filter, working from outside in, is applied to determine the track parameters. In the end, the track is extrapolated to the nominal interaction point and a vertex-constrained fit of the track parameters is performed.

In the global muon reconstruction the muon trajectories are extended to add hits measured by the tracker. The track parameters of a stand-alone reconstructed muon are compared to the track parameters of the tracker tracks by extrapolating the trajectories to a common plane on the inner surface of the muon detector. If a tracker track is found that is compatible in momentum, position and direction, the hit information of the tracker and the muon system is combined and refitted to form a global muon track. The resulting global tracks are then checked for ambiguity and quality to choose at most one global track per stand-alone muon.

The precision of the momentum measurement in the muon system is essentially determined by the measurement of the bending angle in the transverse plane at the exit of the magnetic coil. This measurement is dominated by multiple scattering in the material before the first muon station up to transverse momentum values of 200 GeV. For low-momentum muons the momentum resolution is improved substantially by including the measurement of the silicon tracker. The analysis presented here investigates muons with a transverse momentum between 6 and 30 GeV. The inclusion of the tracker information by using global muons is thus most valuable. In Fig. 2.11 a comparison of the momentum resolution of the muon system, the tracker system and a combined measurement is given for the barrel and the forward region.

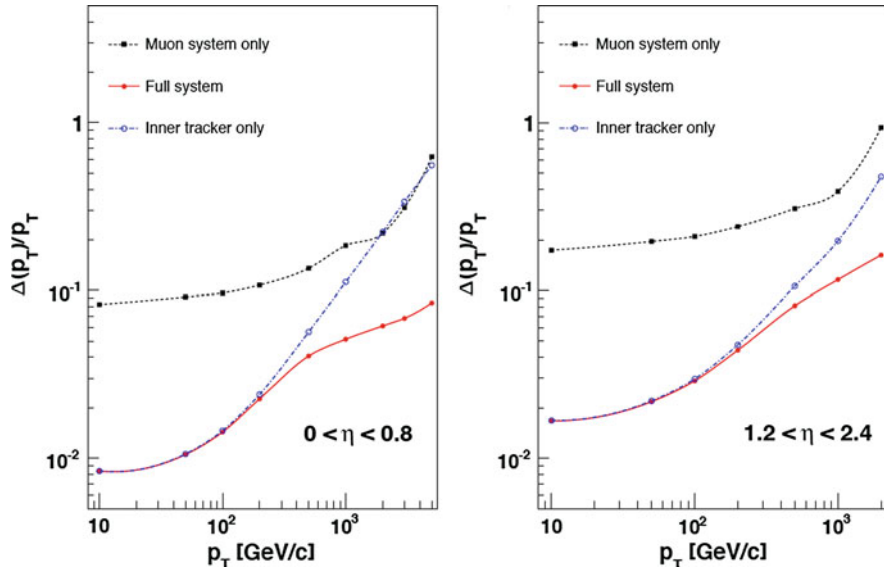


Fig. 2.11 Muon transverse momentum resolution as a function of the transverse momentum for muons detected in the barrel (*left*) and the endcap (*right*) regions [4]. The resolution is given for the measurement using the muon system or the tracking system only and for a combined method

2.2.9 Trigger System

The CMS trigger system is designed to cope with the unprecedented high luminosity and interaction rates. It must ensure high data recording efficiency for a wide variety of physics objects and event topologies, while applying online selective requirements to reduce the 40 MHz event rate to an output rate of about 100 Hz allowing for permanent storage of an event.

The CMS trigger system reduces the event rate in two steps called Level 1 (L1) and High Level Trigger (HLT). The L1 trigger is designed to achieve a maximum output rate of 100 kHz and consists of custom-designed, programmable electronics while the HLT is based on software algorithms running on a large cluster of commercial processors, the event filter farm.

The L1 trigger system uses only coarsely segmented data from the muon system and the calorimeters while the full granularity data are stored in the detector front-end electronics waiting for the L1 decision. The L1 decision has to be taken within a latency time of $3.2 \mu\text{s}$ and is based on the decision of local, regional and global trigger components. It also depends on the readiness of the other subdetectors and the data acquisition system (DAQ) which is supervised by the Trigger Control System. The trigger architecture is displayed in Fig. 2.12.

The ECAL and the HCAL cells form trigger towers with an (η, ϕ) coverage of 0.087×0.087 in $|\eta| < 1.74$ and larger size in the forward region. Trigger primitives

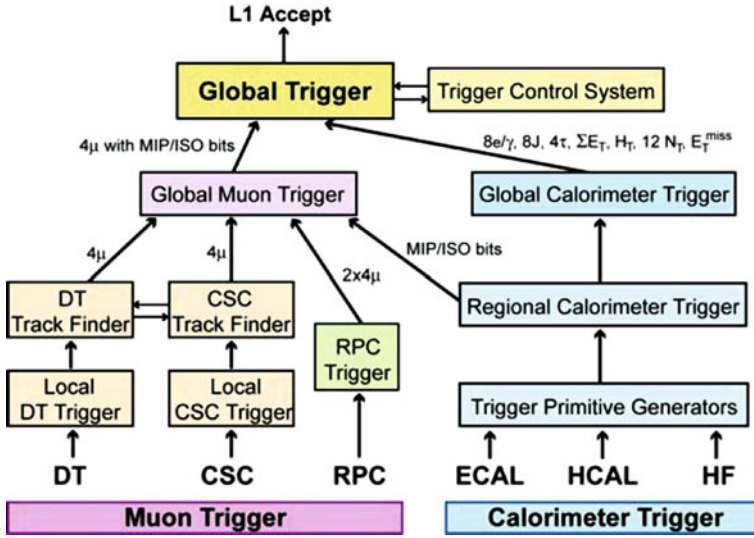


Fig. 2.12 L1 trigger architecture [4]

are generated by calculating the transverse energy of a trigger tower and assigning it to the correct bunch crossing. A regional calorimeter trigger then determines regional electron, photon and jet candidates and information relevant for muon and tau identification. The global calorimeter trigger provides information about the jets, the total transverse energy and the missing energy in the event and identifies the highest-ranking trigger candidates.

In the muon system all three types of detectors take part in the trigger decision. The DT chambers provide track segments in the ϕ projection and hit pattern in η , while the CSC determine three-dimensional track segments. The track finders in the DT chambers and the CSCs calculate the transverse momentum of a track segment and its location and quality. The RPCs deliver an independent measurement derived from regional hit patterns. The global muon trigger receives up to four candidates from each subsystem (DT, barrel RPC, CSC and endcap RPC) together with the isolation information from the global calorimeter trigger. The aim is to improve the efficiency and to reduce the rate by making use of the complementarity and the redundancy of the subsystems. In the end, the global muon trigger selects a maximum of four muon trigger candidates and determines their momentum, charge, position and quality.

The trigger objects extracted by the global calorimeter trigger and the global muon trigger are sent to the global trigger where the decision to accept or reject an event is taken and distributed to the subdetectors. The decision is based on the results of algorithms which for example apply momentum thresholds to single objects or require object multiplicities to exceed predefined values. Up to 128 algorithms can be executed in parallel.

If an event is accepted by the L1 trigger, the full detector information (~ 1 MB) is read out by the DAQ system at a rate of up to 100 kHz, passed to the event filter farm and used as input for the HLT. The HLT algorithms are implemented in the same software as used for offline reconstruction and analysis and consist of subsequent reconstruction and selection steps. The framework uses a modular architecture and the modules to be executed are defined at runtime by means of configuration files. The HLT menu is composed of a set of trigger paths, each path addressing a specific physics object selection. The execution of a path is interrupted if the processed event does not fulfill the conditions imposed by a given filter module. The trigger menu for the first CMS data taking can be found in [9].

References

1. O.E. Brüning et al., LHC Design Report, vol. I: The LHC Main Ring, CERN-2004-003-V-1 (2004)
2. ATLAS Collaboration, Detector and Physics Performance Technical Design Report, vol. 1, CERN-LHCC-99-14 (1999)
3. CMS Collaboration, The Compact Muon Solenoid: Technical Proposal, CERN-LHCC-94-38 (1994)
4. CMS Collaboration, The CMS experiment at the CERN LHC, JINST **3**, S08004 (2008)
5. LHCb Collaboration, LHCb Technical Proposal, CERN-LHCC-98-04 (1998)
6. ALICE Collaboration, Technical Proposal for a Large Ion Collider Experiment at the CERN LHC, CERN-LHCC-95-71 (1995)
7. W. Adam et al., Track Reconstruction in the CMS Tracker, CMS NOTE-2006/041 (2006)
8. P. Billoir, Comput. Phys. Commun. **57**, 390 (1989)
9. CMS Collaboration, CMS High Level Trigger, CERN/LHCC 2007-021 (2007)

Study of the Inclusive Beauty Production at CMS and
Construction and Commissioning of the CMS Pixel Barrel
Detector

Caminada, L.

2012, XIV, 158 p., Hardcover

ISBN: 978-3-642-24561-9